AIAA JOURNAL
Vol. 45, No. 9, September 2007

Aerodynamic Optimization of a Morphing Airfoil Using Energy as an Objective

Howoong Namgoong,* William A. Crossley,† and Anastasios S. Lyrintzis‡
Purdue University, West Lafayette, Indiana 47907-2045

DOI: 10.2514/1.24355

Recent advances in materials science and actuation technologies have raised interest in morphing aircraft that can significantly change shape during flight. The research discussed in this paper focuses upon the shape design of morphing airfoil sections. In the efforts herein, the relative strain energy needed to change from one airfoil shape to another is presented as an additional design objective along with a drag design objective, while constraints are enforced on lift. Solving the resulting multi-objective problem generates a range of morphing airfoil designs that represent the best tradeoffs between aerodynamic performance and morphing energy requirements. From the multi-objective solutions, a designer can select a set of airfoil shapes with a low relative strain energy that requires a small actuation cost and with improved aerodynamic performance at the design conditions.

Nomenclature

C_d	=	coefficient of drag
C_f	=	coefficient of skin friction
C_l	=	coefficient of lift
C_m	=	coefficient of pitching moment
C_p	=	coefficient of pressure
c_j	=	penalty multiplier coefficient
$(EA)_i$	=	axial stiffness of ith linear spring
F_i	=	objective functions
f_i	=	shape functions
k_i	=	spring stiffness coefficient of ith linear spring
L_i	=	undeformed length of ith linear spring
M	=	freestream Mach number
Re	=	Reynolds number
U_{ij}	=	relative strain energy of airfoil i and airfoil j
x	=	x coordinate of airfoil
y	=	y coordinate of airfoil
ΔL_i	=	change in length of ith linear spring
ε_k	=	drag objective function limits
ξ_i	=	design variables
ϕ	=	fitness function

I. Introduction

INVESTIGATIONS of how birds fly have provided inspiration for improved man-made aircraft [1]. Birds can change their wing shape to attain improved maneuverability and maximum performance in different flight conditions. Recently, this wing shape-change ability of birds has led to the concept of a morphing aircraft [2,3]. A morphing aircraft might have deformable airfoil sections that change shape in flight. Several efforts showed that this type of morphing leads to aerodynamic performance benefits for the aircraft [4,5]. The mission adaptive wing (MAW) program [6] of the 1980s demonstrated the aerodynamic performance increases available from a variable camber wing. Despite the aerodynamic advantages, the MAW's variable camber design used on the demonstrator aircraft was impractical due to the increased complexity and weight increase from the actuation system. After the MAW program, most morphing aircraft related research focused on lightweight actuator development to reduce the weight penalty for changing the shape of the aircraft. Examples of recent developments include the Smart Wing [7] and Smart Aircraft and Marine Project System demonstration (SAMPSON) [8] programs; however, many design strategies for morphing aircraft, such as multi-objective optimization including aerodynamic performance and morphing cost (in terms of actuation effort or actuator weight), have not been fully investigated.

The concept of a morphing aircraft introduces the additional aspect of actuation effort that must be addressed in aerodynamic configuration design and optimization. Generally, in developing the objectives for aerodynamic optimization, a multipoint problem formulation [9] is used for airfoil or wing design. A weighted sum of drag coefficients, computed at various design flight conditions, serves as the objective, and constraints ensure that the lift coefficient matches specified values at each of the flight conditions. The resulting shape has performance that is essentially a compromise over the flight conditions. In the case of a morphing aircraft, the wing would be able to change its shape during flight. It should be possible to adjust the wing shape to the best possible shape for any flight condition encountered by the aircraft; this would suggest that the morphing airfoil could be designed using a series of single-point problem formulations. However, there is an actuator effort or "cost" associated with these shape changes. Thus, the effort required to bring about the morphing must be included in the optimization process.

A diverse array of optimization techniques has been applied for traditional aerodynamic design problems. Gradient-based algorithms such as feasible direction [10,11], quasi-Newton [12], and adjoint methods [13] have been widely used for airfoil optimization. Recently, stochastic optimization methods (e.g., genetic algorithms [14,15] and simulated annealing [16]) have been employed for aerodynamic design. These stochastic methods have gained popularity because they perform a global design space search by avoiding local minima that often occur in aerodynamic shape design [17,18]. Work by the authors of this paper also illustrated the presence of local minima in airfoil optimization using a gradient-based search and that a genetic algorithm approach found better performing airfoil shapes with an increased computational cost [19].

The contributions of this paper are the formulation of an energy objective for morphing airfoil design and the application of a multi-objective approach to find tradeoff morphing airfoil designs that minimize both actuator effort and aerodynamic drag. To investigate

Presented as Paper 1324 at the 44th AIAA Aerospace Sciences Meeting and Exhibit, Reno, Nevada, 9–12 January 2006; received 30 March 2006; revision received 4 April 2007; accepted for publication 23 April 2007.

*Graduate Student, School of Aeronautics and Astronautics, 701 West Stadium Avenue; currently Advanced Technologist, Turbine Systems, Rolls-Royce plc, Derby, U.K. Student Member AIAA.

†Associate Professor, School of Aeronautics and Astronautics, 701 West Stadium Avenue. Associate Fellow AIAA.

‡Professor, School of Aeronautics and Astronautics, 701 West Stadium Avenue. Associate Fellow AIAA.

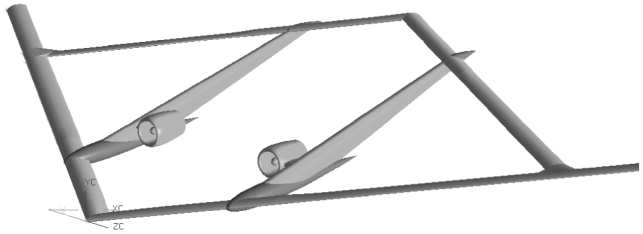

Fig. 1 Notional high-altitude, long-endurance aircraft concept.

energy as an objective for morphing airfoil shape optimization, typical aerodynamics-only design methods and two different multi-objective design methods were applied to a morphing airfoil design. These approaches highlight how strain energy can be included as a measure of the morphing airfoil actuation effort. The results demonstrate the tradeoff between the morphing energy and the aerodynamic performance. Because of the nature of the design problem, a global search method is needed to perform the optimization.

The work of Maute and Reich [20] presents an integrated multidisciplinary topology optimization approach for morphing airfoils that has some similarities to the efforts presented in this paper. In [20], the optimization seeks to describe the internal actuation scheme needed to deform a NACA 0012 airfoil into a shape that maximizes the lift-to-drag ratio of the airfoil for a single flight condition. Constraints on actuator stroke and mechanism mass reflect concerns about the morphing cost. Other efforts for developing morphing shape designs, like that of Lu and Kota [21], use a shape-matching strategy in which the desired shape of the structure is determined in one step, then a subsequent step attempts to design an actuation mechanism that provides the desired shape change. This two-step approach helps define the morphing mechanism but does not directly provide a tradeoff between aerodynamic performance and morphing effort.

II. Representative Problem

Some recent studies by the U.S. Air Force Research Laboratory (AFRL) have focused upon a high-altitude, long-endurance aircraft platform [22]. A notional representation of this concept appears in Fig. 1. This aircraft's design mission includes a 40-hour loiter segment, during which the aircraft experiences a significant weight reduction as it consumes most of its fuel. If the aircraft is intended to loiter at a constant altitude and constant airspeed, a fixed-geometry wing would not be operating at its most efficient conditions throughout this segment of the mission. However, if the aircraft used a wing with morphing airfoil sections, it would be possible to change airfoil shape throughout the loiter segment to improve the aircraft's endurance performance.

Based upon the AFRL studies, required section lift coefficients are known at various times during the long loiter segment. To begin the energy objective investigations, the flight conditions at three points in time during the 40-hour loiter provide the airfoil shape design conditions. Table 1 summarizes these. Near the start of the loiter segment, the aircraft's weight is high, and the required design lift coefficient is also high. Similarly, near the end of the loiter segment, the aircraft's weight is lower, and the lift coefficient is lower. Because of the desire for constant altitude, constant velocity flight, the Reynolds number, and Mach number for all three conditions are the same. The low Mach numbers do not require aerodynamic analyses that include wave drag.

These three flight conditions would only be exactly encountered at three points during the 40-hour loiter; because the aircraft's weight is continuously decreasing, the desired lift coefficient would also continuously decrease. Adding more flight conditions for the morphing airfoil design problem is a possibility, and the multi-objective optimization methodology employed here can accommodate this; however, as will be presented in the following text, this would increase the computational burden. With the three flight conditions, one assumption could be that the morphing airfoil continuously changes between these design shapes, perhaps via a smooth shape transition. With a smooth, continuous shape change, the aircraft will spend about equal time at each flight condition. Another assumption is that the morphing airfoil changes from one discrete shape to another at some point during the 40-hour loiter. At constant loiter speed, and assuming a nearly constant specific fuel consumption of the engine, the aircraft will likely decrease in weight more rapidly near the start of the loiter than near the end of the loiter as the thrust required from the engine decreases. So, with the assumption that the morphing airfoil changes from one discrete shape to another, the aircraft may spend more time close to the low-lift coefficient flight condition than it does close to the high-lift coefficient condition.

Table 1 Airfoil design conditions from 40-hour loiter

	Condition 1	Condition 2	Condition 3
Design C_l	1.52	1.18	0.85
M	0.6	0.6	0.6
Re	1.5×10^6	1.5×10^6	1.5×10^6

III. Aerodynamics Approach

For aerodynamic analysis, the well-known XFOIL [23] code is selected to compute lift and drag coefficients. XFOIL allows for a good resolution of the airfoil shape and is suitable for Reynolds number flows of 1.5×10^6. A linear-vorticity panel method with a Karman–Tsien compressibility correction is used for inviscid calculations. To model viscous effects, source distributions are superimposed on the airfoil and wake. The boundary layer equations are solved together with the inviscid equations by a global Newton method. Although XFOIL is not generally considered a high-fidelity analysis tool, it is relatively fast, a requirement for design studies.

To pose the airfoil shape optimization problem, design variables describing the airfoil shape are needed. Several possibilities were investigated in [24]. The modified Hicks–Henne [25,26] shape functions were found to represent an airfoil most accurately and are used here. The design variables are multipliers that determine the magnitude of the shape function as it is added to the baseline airfoil shape. The y-coordinate positions of the upper and lower surfaces of the airfoil are then described as functions of the x-coordinate position using the following equation:

$$y(x) = y(x)_{\text{base airfoil}} + \sum \xi_i f_i(x) \tag{1}$$

where ξ_i are the design variables and f_i the shape functions. Here, 16 design variables are used ($i = 1, 16$). The first eight govern shape functions applied to the upper surface of the airfoil, and the last eight, the lower surface. Figure 2 provides two plots that depict the shape functions and a NACA 0012 base airfoil along with the upper and lower limits of the airfoil surfaces. The top plot shows how the eight shape functions vary as a function of the chordwise position; this plot uses values $\xi_i = 1.0$. The bottom plot shows the available design space using the NACA 0012 base airfoil with the modified Hicks–Henne shape functions. If all ξ_i are equal to the upper bound of 0.015, the upper bound airfoil shape is described. Similarly, if all ξ_i are equal to the lower bound of -0.015, the lower bound airfoil shape is described. Thus, all possible shapes for the airfoil lie between these two bounds.

IV. Strain Energy as an Objective

As mentioned previously, a morphing airfoil could theoretically provide aerodynamically optimal shapes at any flight condition. However, morphing requires some type of mechanism to effect shape changes. The work described in this paper uses the assumption that the energy needed to change the airfoil shape is proportional to both the actuation system weight and the power needed by the actuation system. The goal of the work in this paper is to account for the extra cost of morphing devices needed to acquire aerodynamic

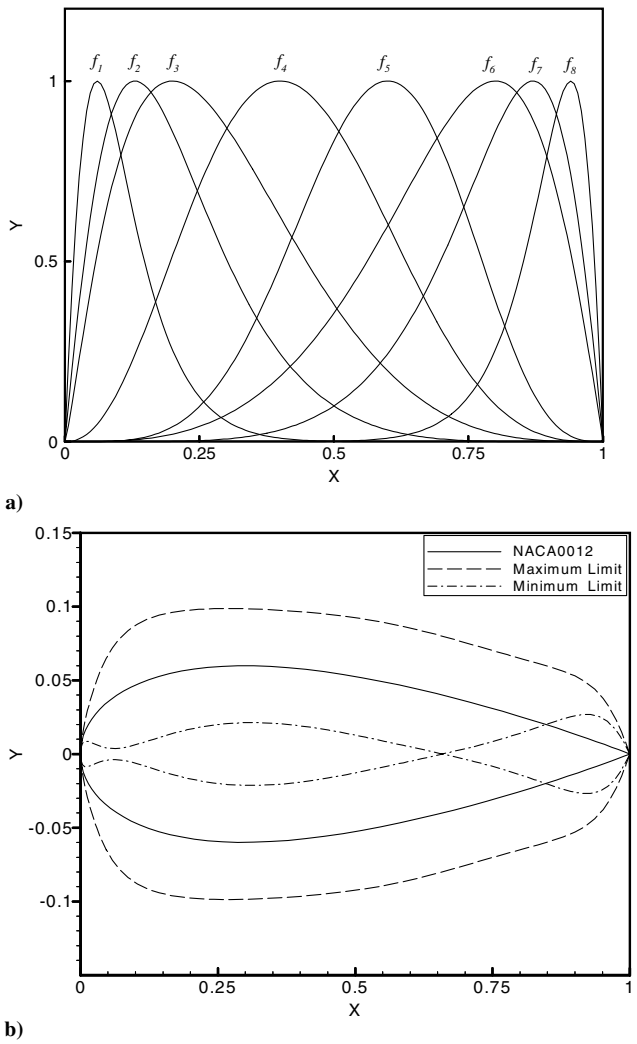

Fig. 2 Modified Hicks–Henne shape functions a) and available design space using the NACA 0012 base airfoil b).

performance benefits. Thus, the additional objective developed here is to minimize the strain energy associated with changing the shape of the airfoil.

There are several ways to model the strain energy needed to change the airfoil shape [27,28]. The basic idea used is that the strain energy in a structure is proportional to the square of the change in length of the structure. In this paper, a simple strain energy model has been considered. This model assumes that springs connect the upper and lower airfoil surfaces to the airfoil's chord line; as the airfoil morphs, the springs deform, which corresponds to an amount of strain energy. Equation (2) presents the linear spring model concept suggested by [27].

$$U = \sum_{i=1}^{n} \frac{1}{2} k_i \Delta L_i^2 = \sum_{i=1}^{n} \frac{1}{2} \frac{(EA)_i}{L_i} \Delta L_i^2 = \sum_{i=1}^{n} \frac{1}{2} (EA)_i \frac{\Delta L_i^2}{L_i} \quad (2)$$

In this equation, U is the strain energy, k_i is the spring constant, $(EA)_i$ is the spring axial stiffness, ΔL_i is the spring deformation, and L_i is the undeformed length of the spring. With no real actuation system envisioned as yet, the spring model strain energy objective does not need to include the stiffness terms $(EA)_i$, so the strain energy objective is the sum of $\Delta L_i^2/L_i$ for all springs used in the model. Figure 3 presents a simple illustration of this model.

The implementation of the linear spring model in this paper relies upon control points identified by XFOIL on the airfoil's surface. Starting with the NACA 0012 base airfoil shape, 141 control points are identified, each with an x/c and a y/c location. The first is the upper surface trailing edge, the 71st is the leading edge, and the 141st

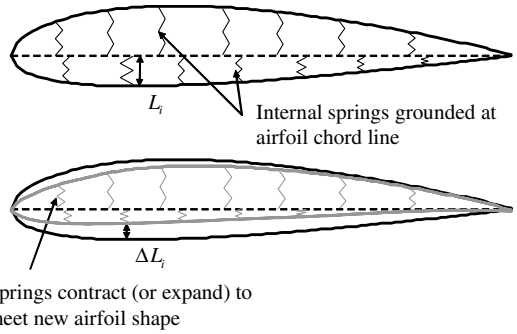

Fig. 3 Internal linear spring model for strain energy.

is the lower surface trailing edge. The leading edge and trailing edge are considered fixed, leaving 138 x/c locations where springs are assumed to connect the chord line with the surface of the airfoil.

To formulate the objective function, relative strain energy terms U_{ij} are introduced representing the strain energy associated with changing from shape i to shape j (e.g., U_{12} indicates energy required to change from shape 1 to shape 2). The objective incorporating strain energy seeks to minimize the maximum relative strain energy value associated with the shape changes. The size and weight of the morphing mechanism is most likely proportional to the peak energy, hence, minimizing the maximum relative energy should minimize the size and weight of the actuator(s). Objective formulations that minimize the sum or an average of the relative energies may not reduce the peak relative energy value. For the three conditions used here, the objective appears as given in Eq. (3).

$$\text{Minimize } [\max(U_{12}, U_{23}, U_{13})] \quad (3)$$

This current strain energy model does not directly account for an actuation or mechanization strategy to change the airfoil shapes. The spring deformation represents all aspects of energy needed to change the airfoil shape, including deformation or shear of the skin covering the airfoil as well as moving or deforming the internal structure. As actuation strategies like those suggested in [21,29,30] become available, models of these strategies should be used to assess strain energy or actuation energy using the optimization framework presented here.

V. Optimization Algorithm

Since its first descriptions, the genetic algorithm (GA) has been applied to many engineering optimization problems. A genetic algorithm is a computational representation of natural selection observed in biological populations [15]. A GA has the ability to search highly multimodal, discontinuous design spaces and, with appropriately selected parameters, can locate designs at or near the global optimum without requiring a good initial design point. Like many global search methods, the GA lacks mathematical proof of convergence to a minimum. If a first-order continuous function could properly represent the morphing mechanism energy and if the airfoil shape problem were definitely unimodal, a calculus-based optimization method could address the morphing airfoil optimization problem. Because the min–max objective formulation for strain energy used here will have discontinuous derivatives [see Eq. (3)] and because airfoil shape design problems appear to frequently have local minima [17–19], the GA provides a search method that would not be hindered by these issues.

There are numerous variations of the genetic algorithm. The GA used here represents individual designs using a binary chromosome coding of the design variable values. Because the morphing airfoil problem has continuous design variables (the shape function multiplier values) and the GA employed here uses binary chromosomes, these design variables are actually discretized to a defined resolution between adjacent values. A tournament selection operator provides the survival of the fittest function. For single-

objective implementations, two designs are chosen at random from the current population, and the one with the better fitness value is copied into the pool of parents for the next generation. For multi-objective implementations, the N-branch tournament [31,32] is used. The N-branch tournament differs from nondominance ranking approaches such as multi-objective genetic algorithm (MOGA) [33], because it uses the selection operator to perform multi-objective design rather than formulation of a single fitness function. New designs are formed using uniform crossover, in which the binary strings of two parent strings are combined to form two child designs by determining which parent string provides the binary value for each child string one bit at a time.

For the single-objective implementations, the GA is halted using a combination of the bit-string affinity (BSA) stopping criterion [34] and a maximum number of generation stopping criterion. The BSA is a measure of similarity of all individuals in a current population. If the binary chromosomes are very similar, the GA can be stopped. A bit-string affinity of 100% would mean that the binary chromosomes of all individuals in the current population were the same. The motivation behind the BSA approach is to ensure a sufficient number of generations for design improvement while avoiding unnecessary effort. The multi-objective implementation seeks a wide range of designs that will have great diversity in the binary chromosomes, so the N-branch tournament GA stops only after a user-defined number of generations.

For the single-objective aerodynamics-only runs and the epsilon-constraint formulation multi-objective runs, the GA evaluated a minimum of 300 generations. If the population's bit-string affinity after the 300th generation exceeded 95%, the GA halted. If the BSA did not exceed 95%, the run continued for additional increments of 25 generations until the population met the BSA criterion. For the multi-objective runs with the N-branch GA, the BSA criterion does not apply because the population is evolving to a diverse set of designs with dissimilar chromosomes, so the GA stops after a specified maximum number of generations (here, 1000).

The population size and mutation rate were selected using empirically derived guidelines [35] for GA using tournament selection and uniform crossover. Seven bits represent each of the 16 shape function multipliers (eight for upper surface and eight for lower surface) in the case of a single airfoil design, for a total chromosome length of 112 bits. For the morphing airfoil design, 48 design variables represent the three shapes, which results in a total chromosome length of 336 bits. The mutation rate is simply the probability that any bit in the child chromosome will be changed to its binary opposite (i.e., from 1 to 0, or from 0 to 1).

The genetic algorithm's selection operator requires a fitness function that reflects the objective function and any constraint violations. For the efforts discussed here, the fitness function was constructed using an external linear penalty function, with the basic form presented in Eq. (4). Values for the penalty coefficients (here, all $c_j = 1.0$) were chosen based on experimentation.

$$\phi(\boldsymbol{\xi}) = F(\boldsymbol{\xi}) + \sum_{j=1}^{n_{\text{con}}} c_j \max[0, g_j(\boldsymbol{\xi})] \tag{4}$$

Using a GA for design optimization can be computationally expensive. Parallelization of the GA overcomes much of the computational time problem. Following the approach of [36], a manager–worker parallelization converted a serial GA into a parallel GA. Because little communication time is needed for the parallel GA, the code scales well [20] on the 104-node Linux Cluster used in this effort. Throughout this study, the computational resources were shared with other users, so the number of processors used varied from 7 to 22.

The computational cost of analyses to compute objective and constraint function values is an issue for any optimization study. Approximations and surrogate models often assist in design optimization where computationally expensive analyses are used; [37,38] are two of the many discussions of these approaches. These surrogate models provide efficient analyses and introduce approximating error. Arguably, the most popular method for surrogate models is the polynomial response surface, in which a least-squares regression finds coefficients of a polynomial function to best fit a series of design analyses conducted before the optimization study.

The largest optimization problems addressed in this study use 48 design variables. A fractional factorial design (e.g., a central composite design) of experiments would require over 2.8×10^{14} function evaluations for this problem. Although the genetic algorithm incurs a significant computational expense, the GA's cost is several orders of magnitude smaller than this. A saturated design for a quadratic response surface—which is not the only surrogate model available, but is widely used—would need 1225 function evaluations. This is far fewer function evaluations than required by the GA. Using this limited set of data to build the surrogate will increase the approximation error.

Alternate sampling strategies and basis functions might be employed so that the number of function evaluations needed to construct the surrogate is on the order of the saturated design and the approximation accuracy is mitigated. However, the authors felt that the work needed to determine appropriate sampling and surrogate modeling for this application was outside the scope of the investigation, given the efficacy of the parallel GA. The identification and implementation of appropriate surrogate models would provide a rich opportunity for further study and could make multi-objective study of morphing airfoils more efficient.

VI. Investigations and Results

Two typical aerodynamics-only design problems and the newly suggested energy-based multi-objective design are investigated. The aerodynamics-only problems provide the extremes of the tradeoff between low drag and low strain energy.

The design variables are used to describe the airfoil shape as shown in Eq. (1). For the single-point and multipoint aerodynamics-only designs, 16 design variables are needed. In the cases using strain energy as an objective, a total of 48 design variables (16 for each of the three flight conditions) are needed to describe shapes for each design condition. The NACA 0012 airfoil is selected as a base airfoil for all shapes. The same modified Hicks–Henne shape functions and design variable bounds ($\xi_i = \pm 0.015$) that were described previously are used here. Thus, the same limits on upper and lower surface shapes shown in Fig. 2 are provided. This range of design variables could include shapes where the upper and lower surfaces are crossed. If a shape is encountered where the surfaces cross, the airfoil is not analyzed by XFOIL; instead, it is assigned an arbitrarily large fitness function value so that it will not survive the selection operator in the genetic algorithm.

In optimal airfoil shape design, the angle of attack also can be, and often is, used as one of the design variables, so that the solution contains the shape and angle of attack needed to minimize drag and meet the lift constraints. However, in this research, the angle of attack was not a design variable, because XFOIL has a built-in trimming subroutine to find the angle of attack that satisfies the design lift constraint. This internal trimming routine uses a maximum of 20 iterations with a tolerance of 1×10^{-6}. For airfoils evaluated in this study, the trimming routine always found the angle of attack necessary to meet the design lift coefficient. Using XFOIL's trimming process reduces the number of design variables, which reduces the complexity of the design space making it easier to find a near-global optimum design. Also, using trimming instead of treating the angle of attack as a design variable can avoid the possibility that two different airfoil shapes at different angles of attack have nearly the same fitness function value, because each evaluated airfoil is at the necessary angle of attack to meet the lift coefficient.

XFOIL uses inviscid calculations in the trimming procedure; then it predicts an airfoil's drag coefficient using the viscous boundary layer calculations. At high angles of attack, some poor airfoil shapes can create problems for XFOIL's viscous boundary layer solver. To address this, a constraint enforces feasible airfoil shapes to have a

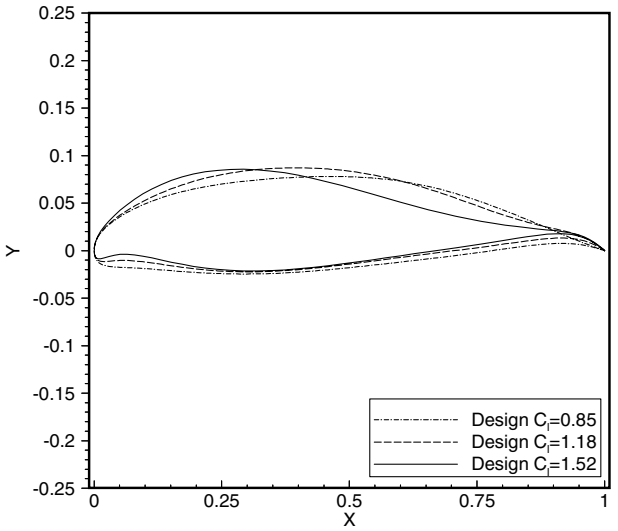

Fig. 4 Airfoil shapes from single-point optimizations.

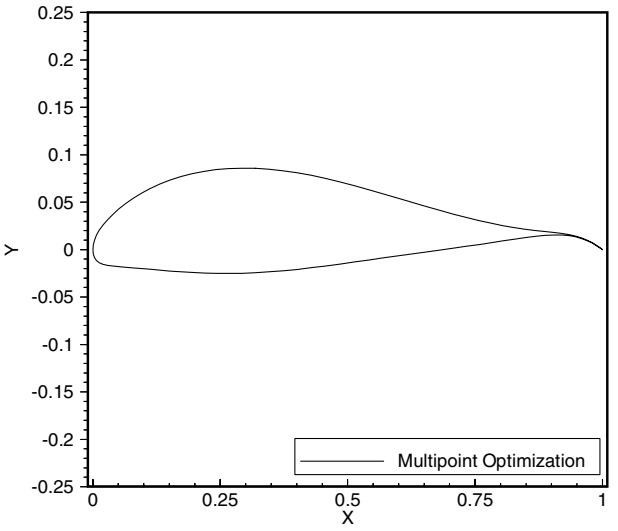

Fig. 5 Airfoil shape from multipoint optimizations.

residual error from XFOIL's viscous boundary layer solution that is below a specified tolerance.

A. Aerodynamics-Only Investigation

1. *Three Single-Point Airfoil Designs*

With no consideration of the energy needed to change the morphing airfoil's shape, the airfoil would be able to adjust so that its performance at any given flight condition would match the result of a single-point optimization at that flight condition. Each problem results in a single shape that minimizes C_d at each condition. Equation (5) shows the single-point problem objective that corresponds to each of the flight conditions ($k = 1, 2, 3$). The lift coefficient constraints are satisfied by trimming the airfoil, so an explicit constraint is unnecessary. The viscous solver residual error δ_{solver} is acceptable if it is less than or equal to 0.002.

$$\text{Minimize } F(\boldsymbol{\xi}) = C_{d_k}(\boldsymbol{\xi}) \tag{5}$$

$$\text{Subject to } g_1(\boldsymbol{\xi}) = \delta_{\text{solver}}(\boldsymbol{\xi}) - 0.002 \leq 0 \tag{6}$$

$$-0.015 \leq \xi_i \leq 0.015 \qquad i = 1, 16 \tag{7}$$

For this 16-variable problem with a corresponding chromosome length of 112 bits, the population size is 448 individuals, and the mutation rate is 0.0022 following the aforementioned guidelines [35]. In Fig. 4, the resulting airfoils from the three single-point optimization runs are superimposed on each other to demonstrate the type of shape changes that would be required for morphing the airfoil to meet the three flight conditions given in Table 1. These represent the best possible aerodynamic shapes for the airfoils.

These runs each required 300 generations, and each fitness evaluation required one XFOIL solution, for a total of 134,400 XFOIL solutions. Each of these runs used seven CPUs on the computing cluster; the elapsed times for these runs were 10,553 s (176 min) for the C_{l1} condition; 17,360 s (289 min) for the C_{l2} condition; and 14,173 s (236 min) for the C_{l3} condition.

2. *Multipoint Optimization*

The multipoint approach uses the weighted sum of drag coefficients shown in Eq. (8) as the objective function, following a typical formulation for this problem type [9]. Equal weights for the drag coefficients in Eq. (8) reflect the assumption the aircraft will spend nearly equal time at each flight condition during the loiter segment. This approach finds a single, fixed-geometry shape that compromises between all three flight conditions. The lift coefficient constraints are satisfied by trimming the airfoil; shapes that encounter poor boundary layer solutions for any of the three flight conditions will violate one of the tolerance constraints:

$$\text{minimize } F(\boldsymbol{\xi}) = \frac{C_{d_1}(\boldsymbol{\xi})}{3} + \frac{C_{d_2}(\boldsymbol{\xi})}{3} + \frac{C_{d_3}(\boldsymbol{\xi})}{3} \tag{8}$$

$$\text{subject to } g_1(\boldsymbol{\xi}) = \delta_{\text{solver}_1}(\boldsymbol{\xi}) - 0.002 \leq 0 \tag{9}$$

$$g_2(\boldsymbol{\xi}) = \delta_{\text{solver}_2}(\boldsymbol{\xi}) - 0.002 \leq 0 \tag{10}$$

$$g_3(\boldsymbol{\xi}) = \delta_{\text{solver}_3}(\boldsymbol{\xi}) - 0.002 \leq 0 \tag{11}$$

$$-0.015 \leq \xi_i \leq 0.015 \qquad i = 1, 16 \tag{12}$$

This problem also has 16 variables, so the corresponding population size and mutation rate are 448 and 0.0022, respectively [35]. The result is an airfoil with higher drag at each specific flight condition compared to the corresponding single-point optimized airfoils. Because a single airfoil shape is acquired by this approach, the airfoil requires no strain energy. Figure 5 presents the resulting single airfoil shape.

Results of the two aerodynamics-only problem formulations are compared in Table 2. The single-point design results have lower drag than the multipoint design results, as expected. This is because the single-point designs have only one objective, which is to minimize drag at one flight condition, but the multipoint design solution is a compromise solution over all three flight conditions. The relative strain energies in Table 2 are all zero for the multipoint design. The relative energies shown in Table 2 for the single-point solutions are calculated using the energy model described in Eq. (2). Therefore, the values in Table 2 indicate the range of tradeoff available for a morphing airfoil. The three single-point shapes are the best aerodynamic solution, while the multipoint shape is the best energy solution.

The multipoint run required three XFOIL solutions for each fitness evaluation. The GA ended its run after 300 generations and used 403,200 XFOIL analyses. With 12 CPUs, the wall clock time for this run was 34,641 s (577 min or 9.6 h).

Table 2 Drag and energy comparison of aerodynamics-only designs

	Single point	Multipoint
C_{d_1}	0.010249	0.010649
C_{d_2}	0.007015	0.008178
C_{d_3}	0.005024	0.007356
U_{12}	0.00704	0
U_{23}	0.00189	0
U_{13}	0.01241	0

B. Energy-Based Investigation

In the design approach used here, strain energy is proposed as another objective to encourage minimum actuation requirements for morphing airfoils. Because the aerodynamic performance also needs to be included, the problem becomes multi-objective. For the multi-objective optimization, the objective function may be considered a vector function whose components are individual objectives. In a problem with more than one competing objective, there exist a number of solutions called the Pareto-optimal set [39], instead of a single best solution. This research employs two multi-objective methods (i.e., ε constraint and N-branch tournament genetic algorithm [31,32]) to address the two objectives: strain energy and drag.

1. ε-Constraint Approach

In the ε-constraint approach, one of the original objective functions is converted to a constraint, and the other objective is minimized. Here, the drag objective is converted to a constraint, and this constraint is enforced in the GA via a penalty function. The drag objective function limit values (ε_k) are chosen between the values associated with the single-point and multipoint results in Table 2. By varying the values of ε_k for different runs of the optimizer, different Pareto-optimal solutions are found. Thus, this approach always finds an aerodynamically better shape than the multipoint aerodynamics-only design. The formulation of the ε-constraint approach is described in Eq. (14). The coefficients C_1 and C_2 provide numerical scaling and both are equal to 0.01 here. As with the previous problems, the lift coefficient constraints are satisfied via trimming, and shapes with a poor boundary layer calculation will violate a solver tolerance constraint.

$$\text{Minimize } F_1(\boldsymbol{\xi}) = \frac{1}{C_1}\max[U_{12}(\boldsymbol{\xi}), U_{23}(\boldsymbol{\xi}), U_{13}(\boldsymbol{\xi})] \tag{13}$$

$$\text{Subject to } g_1(\boldsymbol{\xi}) = \frac{1}{C_2}\left[\frac{C_{d_1}(\boldsymbol{\xi})}{3} + \frac{C_{d_2}(\boldsymbol{\xi})}{3} + \frac{C_{d_3}(\boldsymbol{\xi})}{3}\right] \le \varepsilon_k \tag{14}$$

$$g_2(\boldsymbol{\xi}) = \delta_{\text{solver}_1}(\boldsymbol{\xi}) - 0.002 \le 0 \tag{15}$$

$$g_3(\boldsymbol{\xi}) = \delta_{\text{solver}_2}(\boldsymbol{\xi}) - 0.002 \le 0 \tag{16}$$

$$g_4(\boldsymbol{\xi}) = \delta_{\text{solver}_3}(\boldsymbol{\xi}) - 0.002 \le 0 \tag{17}$$

$$-0.015 \le \xi_i \le 0.015 \qquad i = 1, 16 \tag{18}$$

Seven different values of ε_k (0.856, 0.840, 0.824, 0.807, 0.791, 0.775, and 0.759) constrained the drag objective function. For each value of ε_k, the problem has 48 variables, and the GA uses 336-bit chromosomes to represent each individual design. With this chromosome length, the population size for these runs was 1344 individuals, and the mutation rate was 0.00037 (using [35]). Each fitness evaluation for these runs required three XFOIL analyses, and each GA run in the ε-constraint approach completed 400 generations. This corresponds to a total 1,612,800 XFOIL solutions for each run. To complete all seven runs, the GA conducted 11,289,600 XFOIL solutions. Each of the seven runs used between 12 and 22 CPUs from the cluster, and the wall clock times for these runs varied between 137,282 s (2288 min or 38.1 h) and 159,923 s (2665 min or 44.4 h).

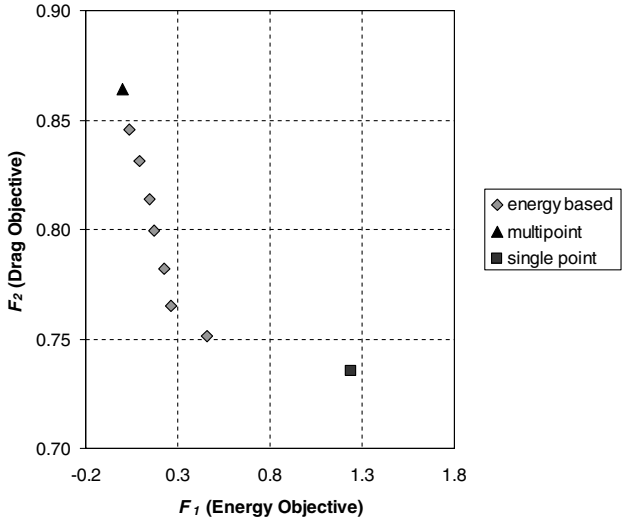

Fig. 6 Pareto set from ε-constraint approach.

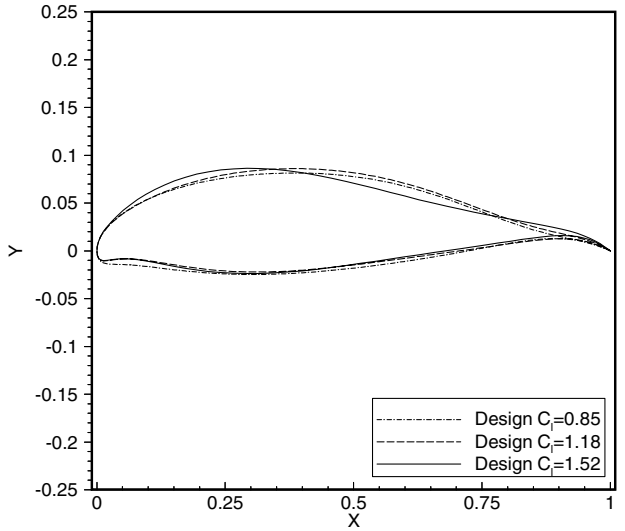

Fig. 7 Selected morphing airfoil shape set from multi-objective design (ε-constraint approach).

Figure 6 shows the Pareto set of seven "energy-based" points found from the ε-constraint approach that include the energy objective function in the multi-objective problem. The single-point and multipoint aerodynamic-only designs also appear in Fig. 6 for comparison with the multi-objective results. The energy-based points represent the tradeoff morphing airfoil solutions between the two extreme points represented by the aerodynamics-only solutions.

Figure 7 shows the set of three shapes associated with one morphing airfoil tradeoff solution selected from the Pareto-optimal set. This airfoil set has a lower drag objective function value than the multipoint design and also has a smaller strain energy objective function value than the single-point design. The morphing airfoil set in Fig. 7 has a drag objective of 0.765, which is lower than the multipoint airfoil's drag objective of 0.864. Also, the morphing airfoil in Fig. 7 has an energy objective of 0.260, which is lower than that of the set of single-point shapes at 1.240. This airfoil set shows little shape change in the lower surface to reduce energy but has more

variation in the upper surface to maintain the required C_l values with low drag.

2. N-Branch Tournament Genetic Algorithm

Many different modifications of the genetic algorithm have been used for multi-objective optimization. An appropriately modified GA can generate a large number of designs that represent the Pareto set for a multi-objective problem with computational effort similar to that required to solve a single-objective problem with a GA. Equation (19) presents the vector-valued objective for this optimization. The N-branch tournament [31] is used here to generate a representation of the Pareto set. This creates two fitness functions: one associated with the drag objective and one with the energy objective. The airfoil trimming procedure enforces the equality constraints on C_l, and tolerance constraints address airfoils with poor boundary layer solutions using Eqs. (9–11) above.

$$\text{Minimize } \mathbf{F}(\boldsymbol{\xi}) = \left\{ \begin{array}{c} \frac{1}{C_1}\max[U_{12}(\boldsymbol{\xi}), U_{23}(\boldsymbol{\xi}), U_{13}(\boldsymbol{\xi})] \\ \frac{1}{C_2}\left[\frac{C_{d_1}(\boldsymbol{\xi})}{3} + \frac{C_{d_2}(\boldsymbol{\xi})}{3} + \frac{C_{d_3}(\boldsymbol{\xi})}{3}\right] \end{array} \right\} \tag{19}$$

$$-0.015 \le \xi_i \le 0.015 \qquad i = 1, 48 \tag{20}$$

This multi-objective problem has 48 design variables, so the GA uses 336-bit chromosomes. The corresponding population size is 1344 individuals, and the corresponding mutation rate is 0.00037 (using [35]). Figure 8 shows the Pareto set found from one run (1000 generations) of the N-branch tournament GA. The representation of the Pareto set was assumed to be converged after 1000 iterations; few changes were observed in the Pareto set after about 800 generations. Each fitness evaluation used results from three XFOIL solutions, so the N-branch tournament GA conducted 4,035,000 XFOIL analyses. Using 12 CPUs, the wall clock time for this run was 106,313 s (1772 min or 29.5 h). The N-branch tournament GA found 163 nondominated morphing airfoil designs with just over 4×10^6 XFOIL solutions, while the ε-constraint formulation required over 11×10^6 XFOIL solutions to find only seven nondominated designs.

Figure 9 is one of the tradeoff solutions selected from the Pareto set shown in Fig. 8. The morphing airfoil in Fig. 9 has a drag objective of 0.765 and energy objective of 0.2. The morphing airfoil shapes in Figs. 7 and 9 seem similar, but the energy objective of the airfoil shapes in Fig. 9 is slightly lower. The airfoil shapes in Fig. 9 are much closer to each other than the single-point generated airfoil shapes in Fig. 4, which follows that the strain energy of the morphing airfoil in Fig. 9 is smaller than that associated with the three single-point shapes.

Figures 10–12 present airfoil shapes and C_p distributions associated with the three flight conditions. The top plots show the single-point shape designed for the given flight condition, the multipoint shape, a morphing airfoil shape obtained via the ε-constraint method for the given flight condition (see Fig. 7), and the morphing airfoil shape obtained via the N-branch GA for the given flight condition (see Fig. 9). The airfoil shapes generated using the multi-objective approaches lie between the two aerodynamics-only designs, showing the compromise between the low-energy objective, which would require small shape changes, and a low drag objective, which would require large shape changes.

One noticeable trend from the airfoil and C_p comparison is that the differences among the shapes decrease as the design C_l increases. This can be attributed to the fact that for the high C_l design condition, airfoils that satisfy the high C_l with low drag without approaching stall (recall that airfoils near stall can create viscous convergence problems for XFOIL) are hard to find. The trailing edge of all the airfoils has become quite thin, which would require additional consideration if the airfoils were to be manufactured. Airfoil shapes at the highest C_l design condition have the thinnest trailing edges.

Figure 8 presented the representation of the Pareto-optimal set, as generated by the N-branch tournament GA. As with any multi-objective GA, the N-branch tournament's representation of the Pareto set is not exact. The multipoint, aerodynamics-only solution indicates the low-energy, high-drag end of the Pareto set. The N-branch GA's representative Pareto set generates designs that are very close to the multipoint, aerodynamics-only solution; however, the representative Pareto set does not pass through this design. The multipoint, aerodynamics-only design problem, by definition requires no energy. For a multi-objective result to match the multipoint, aerodynamics-only design, the N-branch GA must generate a binary string where the set of 16 variables representing the first design condition shape, the set of 16 variables representing the second design condition shape, and the set of 16 variables representing the third design condition shape must be exactly the same (i.e., $\xi_1 = \xi_{17} = x_{33}, \xi_2 = \xi_{18} = \xi_{34}, \ldots, \xi_{16} = \xi_{32} = \xi_{48}$). Comparing designs from the low-energy, high-drag end of the representative Pareto set to the multipoint, aerodynamics-only design suggests that there is very little difference in these designs. These minor differences are indicative of how the N-branch GA represents the Pareto frontier for this problem and is analogous to finding near-global optima in single-objective problems.

Although many nondominated morphing airfoil designs are included in this representation of the Pareto frontier, there is a notable lack of designs in the low-drag, high-energy region of the front, where the drag objective is below 0.74 and the energy objective is

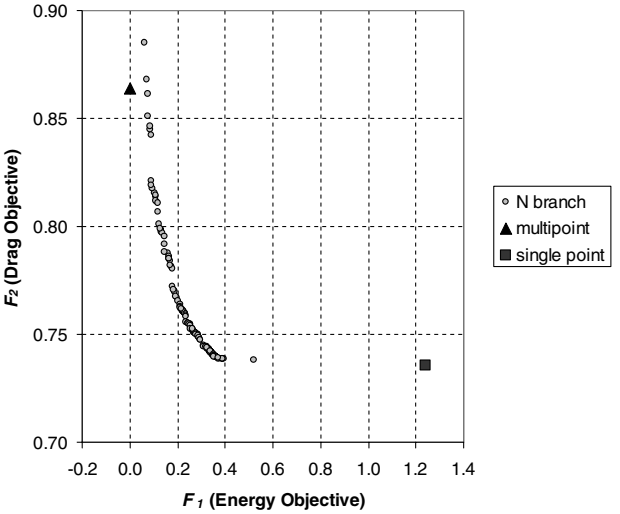

Fig. 8 Pareto set from N-branch tournament GA.

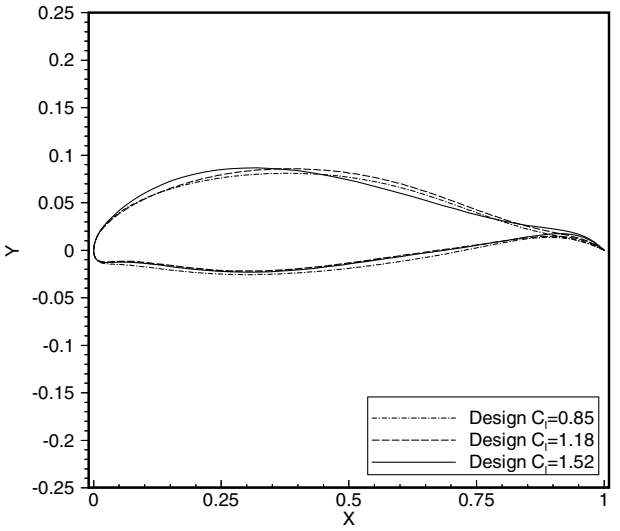

Fig. 9 Selected morphing airfoil shape set from multi-objective design (N-branch tournament GA).

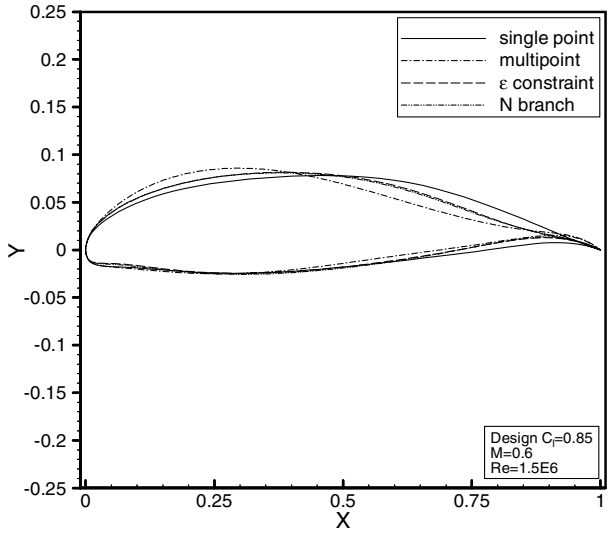

a)

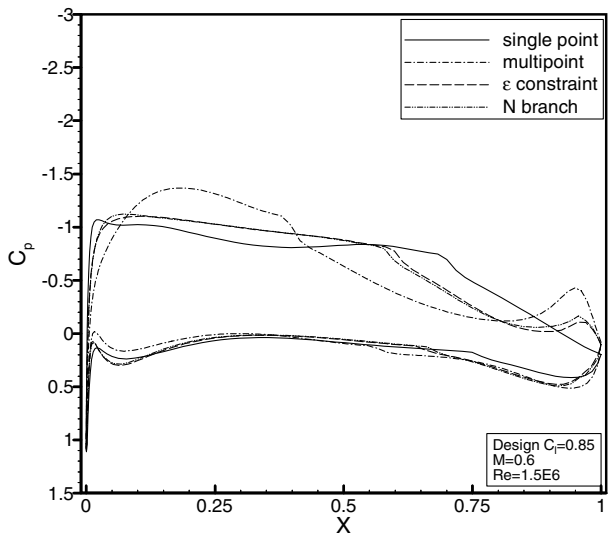

b)

Fig. 10 Airfoil comparison a); C_p distribution comparison b) (design $C_l = 0.85$).

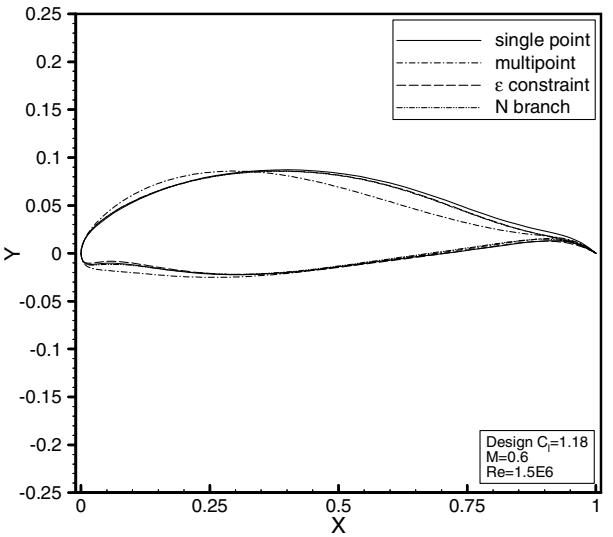

a)

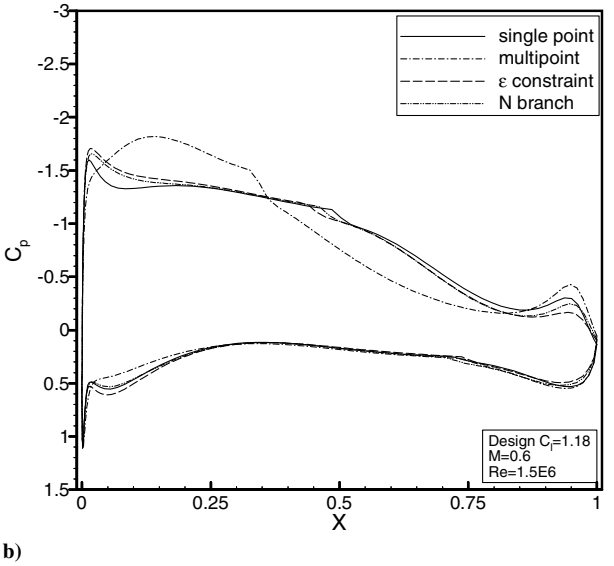

b)

Fig. 11 Airfoil comparison a); C_p distribution comparison b) (design $C_l = 1.18$).

above 0.4. Features of the problem, in addition to the approximating nature of the N-branch GA's representation of the Pareto frontier, appear responsible for this gap. The set of single-point shapes should indicate the low-drag, high-energy end of the Pareto front. Attempts were made to identify multi-objective solutions in this region of the front by using the ε-constraint approach with smaller limits on the drag objective than previously used and by using the ε-constraint approach to minimize drag with limits on the energy objective. No feasible morphing airfoil designs between the set of single-point shapes and the nondominated designs in Fig. 8 could be found via these approaches. Three features appear to be responsible for this gap in the Pareto front.

The first is associated with the predicted aerodynamic performance. The aforementioned difficulty in finding shapes for the high C_l design condition limits the possible solutions. The drag associated with feasible shapes at this condition is substantial and difficult to reduce without violating the solver tolerance constraint [Eq. (15)]. As a result, the morphing airfoil and the single-point airfoil for $C_l = 1.52$ in Fig. 12 have nearly the same shape, nearly the same C_P distribution, and nearly the same predicted C_d (0.01044 for the morphing airfoil and 0.01025 for the single-point airfoil). The aerodynamic analysis used here predicts viscous drag using an integral boundary layer calculation that includes an estimation of boundary layer transition from laminar to turbulent. At the $C_l = 1.52$ flight condition, the boundary layer of the morphing airfoil shape in Fig. 9 transitions from laminar to turbulent at 0.26 x/c on the upper surface and at 0.79 x/c on the lower surface; similarly, the boundary layer for the single-point airfoil at $C_l = 1.52$ transitions at 0.26 x/c and 0.80 x/c on the upper and lower surfaces, respectively. For the $C_l = 0.85$ design condition, the morphing airfoil shape in Fig. 10 has a drag coefficient of 0.00567 and predicted boundary layer transition locations of 0.57 x/c and 0.66 x/c for the upper and lower surfaces. The single-point airfoil in Fig. 10 for $C_l = 0.85$ has a C_d of 0.00503 and predicted boundary layer transition locations of 0.69 x/c and 0.74 x/c. At this lower lift design condition, the predicted transition location has an important impact on the drag coefficient, and it appears that moving from the lowest-drag objective morphing airfoil in Fig. 8 toward the end of the Pareto front represented by the single-point shapes requires only a minor change in prediction of the boundary layer transition location. A very minor change in the airfoil shape could create this type of minor change in boundary layer transition prediction.

The second feature is related to the problem formulations and design variable representation. The multi-objective problem uses 48 design variables, while each of the three single-point design problems uses 16 design variables. This reduction in the number of design variables makes it somewhat easier to find low-drag shapes in the single-point formulation. Further, a small change in the shape of

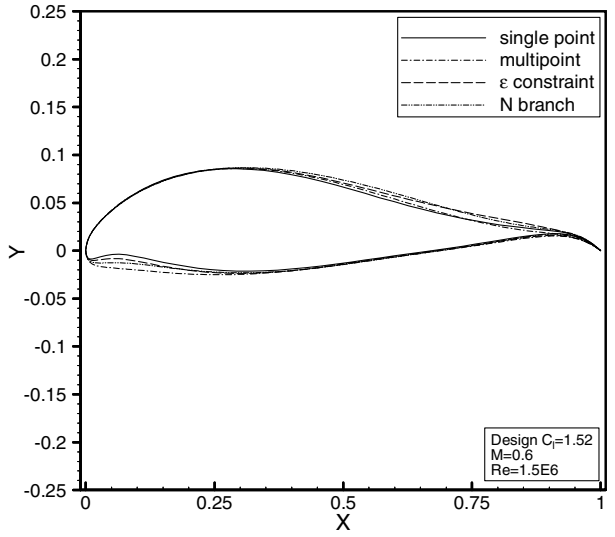

a)

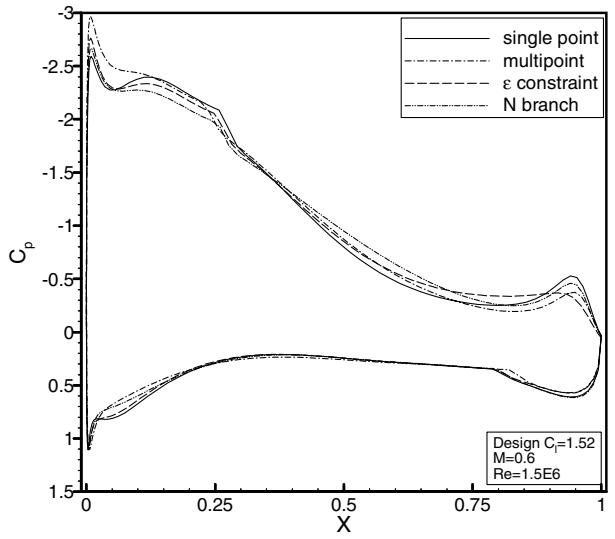

b)

Fig. 12 Airfoil comparison a); C_p distribution comparison b) (design $C_l = 1.52$).

the airfoil can lead to a change in the boundary layer transition location as just described. If only a very few bits out of the 336 in the chromosome string representing the lowest-drag objective morphing airfoil design from the *N*-branch GA must change to find a lower-drag, higher-energy morphing airfoil, obtaining that small change via the GA is difficult.

The third feature is the necessity of handling designs with crossed upper and lower surfaces with an arbitrarily large fitness function that may be eliminating features from the GA population that are needed to further reduce drag in the multi-objective problem formulation. The thin trailing edges of the airfoil shapes, particularly at the high-lift design condition, suggest this may be a possibility. So, even if a few of the 336 bits in the chromosome need to be different from the lowest-drag objective morphing airfoil for a lower-drag, higher-energy solution, the proper pattern of ones and zeros to achieve this may not survive in the GA's population if they are often associated with physically unrealizable airfoil shapes.

In the linear spring strain energy model, the springs are assumed to connect a control point on the airfoil's surface to the centerline of the airfoil. With this in mind, Figs. 13–15 present the relative strain energy in each spring that results when changing from one shape to another. The NACA 0012 shape is used in these figures solely for clarity, This allows the energy associated with a spring connecting any given control point to the centerline to appear in the same location in these plots, regardless of the final shapes obtained from

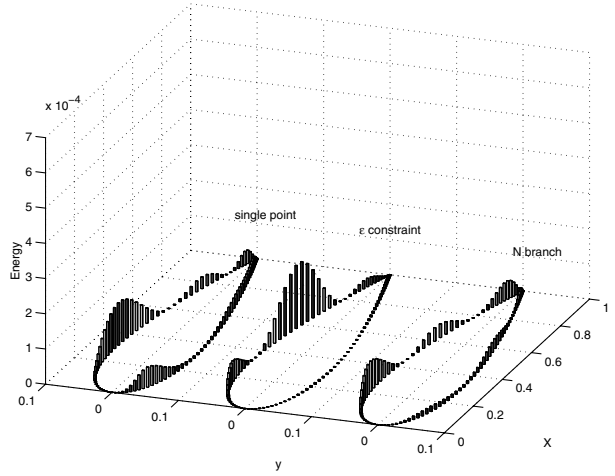

Fig. 13 Strain energy distributions (U_{12}).

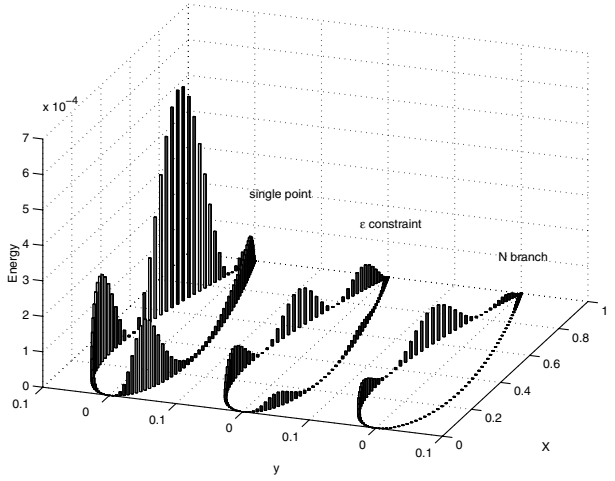

Fig. 14 Strain energy distributions (U_{23}).

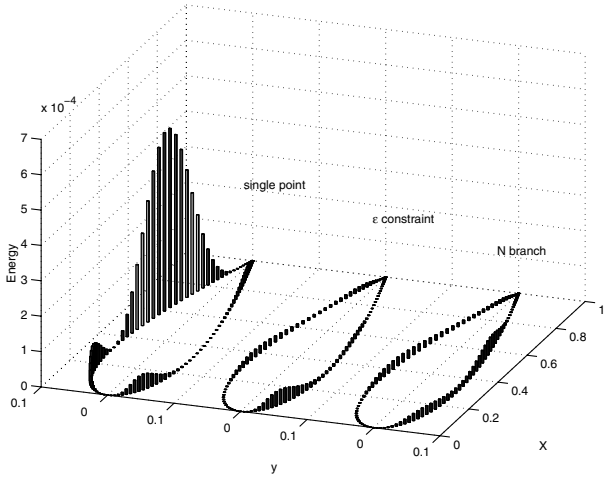

Fig. 15 Strain energy distributions (U_{13}).

the set of single-point solutions, from the ε-constraint approach, or from the *N*-branch tournament approach. In these plots, if the spring associated with a control point has a large displacement between two airfoil shapes, a large bar is placed at the corresponding control point on the NACA 0012 airfoil section. In this manner, the visual representation shows which section of the airfoil is associated with the highest strain energy.

The set of single-point shapes was generated without any concern for strain energy, so many of the springs deform significantly when moving from one of the single-point shapes to another. This is particularly obvious in Figs. 14 and 15, which show that the relative strain energy values U_{23} and U_{13} are very large in springs on the upper surface of the airfoil. With strain energy as part of the multi-objective problem, the spring deformations are much smaller, as is expected from the energy objective, which seeks to minimize the sum of $\Delta L_i/L_i$. With this strain energy included as an objective, the resulting morphing airfoil shapes have very little change in the lower surface, which results in very low energy in springs along the lower surface. When changes are needed to improve drag at each flight condition, these changes largely occur on the upper surface of the airfoil. If other morphing schemes providing large deformations from little input energy become available, there may be larger changes in shape between the three morphing flight conditions. Regardless of the morphing scheme, the multi-objective approach demonstrated here can still determine appropriate tradeoffs between morphing effort and aerodynamic performance.

C. Drag Objective Discussion

The multipoint formulations of the drag objective in the multipoint, aerodynamics-only and in the multi-objective optimization studies used equal weights to modify the drag coefficients at each of the three flight conditions in Table 1. To get a sense of how changing the drag objective formulation could impact the resulting airfoil shapes, the three alternate drag objective formulations shown in Eqs. (21–23) generated airfoil shapes using the multipoint, aerodynamics-only problem formulation.

$$\text{Minimize } F(\boldsymbol{\xi}) = \frac{2C_{d_1}(\boldsymbol{\xi})}{9} + \frac{3C_{d_2}(\boldsymbol{\xi})}{9} + \frac{4C_{d_3}(\boldsymbol{\xi})}{9} \tag{21}$$

$$\text{Minimize } F(\boldsymbol{\xi}) = \frac{3C_{d_1}(\boldsymbol{\xi})}{12} + \frac{4C_{d_2}(\boldsymbol{\xi})}{12} + \frac{5C_{d_3}(\boldsymbol{\xi})}{12} \tag{22}$$

$$\text{Minimize } F(\boldsymbol{\xi}) = \frac{C_{d_1}(\boldsymbol{\xi})}{3(C_{d_1})_{\text{sp}}} + \frac{C_{d_2}(\boldsymbol{\xi})}{3(C_{d_2})_{\text{sp}}} + \frac{C_{d_3}(\boldsymbol{\xi})}{3(C_{d_3})_{\text{sp}}} \tag{23}$$

Equations (21) and (22) provide a higher weighting toward the third flight condition. If the morphing airfoil scheme requires that the wing section change discretely between the three shapes, the aircraft will spend more time near this flight condition. The formulation in Eq. (23) uses information from the three single-point shape runs, denoted as $(C_{di})_{\text{sp}}$, to truly give each flight condition equal consideration in the drag objective function. The drag objective used in the studies discussed in the previous subsections [Eqs. (8), (14), and (19)] used equal weights, but did not normalize the drag coefficients.

Table 3 presents information about the resulting airfoils obtained for the multipoint, aerodynamics-only problem using Eqs. (8) and (21–23). Also appearing in Table 3 is the percentage that each flight condition contributes to the drag objective function at the solution. The first flight condition dominates the equal-weighting scheme of Eq. (8). The weighting scheme of Eq. (21) results in a morphing airfoil design where the drag coefficient associated with the third flight condition provides the largest contribution to the objective function. The weighted sum of Eq. (22) and the sum of equally weighted normalized drag coefficients of Eq. (23) generate morphing airfoil designs with objective functions that receive nearly equal contribution from all three flight conditions. The multipoint airfoil design generated using Eq. (23) has the highest C_{d1} value and lowest C_{d3} value of all formulations in the table. Clearly, the formulation of the objective function affects the resulting morphing airfoil designs.

The formulation of the drag objective used in a multi-objective design study of morphing airfoils should consider the morphing mechanism and strategy. If the morphing mechanism can provide a continuous, smooth shape change, perhaps the equal-weighting objective or the normalized drag coefficient objective best represents the design goals. If the morphing mechanism provides discrete shape changes, perhaps an appropriate objective function weights the drag coefficient terms based upon length of time flown at or near the associated flight conditions. In any case, the multi-objective approach for designing morphing airfoils presented here will indicate the amount of tradeoff that exists between aerodynamic improvement and energy required for the shape change.

Table 3 Impact of alternate drag objective formulations on multipoint aerodynamics-only results

	Eq. (8)	Eq. (21)	Eq. (22)	Eq. (23)
C_{d_1}	0.010649	0.011164	0.011602	0.011982
C_{d_2}	0.008178	0.008460	0.008524	0.008141
C_{d_3}	0.007357	0.007222	0.007268	0.006378
$F(\boldsymbol{\xi}^*)$	0.008728	0.008511	0.008770	1.199738
C_{d_1} contrib.	40.7%	29.2%	33.1%	32.5%
C_{d_2} contrib.	31.2%	33.1%	32.4%	32.2%
C_{d_3} contrib.	28.1%	37.7%	34.5%	35.3%

The XFOIL analysis tool provided the drag coefficient predictions for the studies described above. Features of the drag prediction associated with boundary layer transition and shapes that do not allow for boundary layer solutions at high C_l might suggest that the study would benefit from a higher-fidelity aerodynamic analysis. Additionally, many discussed applications of morphing aircraft include dissimilar flight regimes in which not only would C_l change across flight conditions, but the Mach and Reynolds numbers would also vary. Transonic design conditions require higher-fidelity analyses than XFOIL as well. Preliminary studies [24] that replaced XFOIL with a higher-fidelity Navier–Stokes code for transonic morphing airfoil design required a significant increase in computational effort, but indicated that the same multi-objective approach of the N-branch tournament GA can effectively generate many minimum-drag, minimum-energy designs representing the Pareto set.

VII. Conclusions

Design of a morphing airfoil must consider both the aerodynamic performance gained from changing the airfoil's shape and the effort necessary to actuate the shape change. The shape change can improve the aerodynamic performance of the airfoil over that of a fixed airfoil shape. However, the actuation energy of the morphing airfoil will be proportional to the power and weight of the morphing mechanisms; this additional weight and power could negate the impact of the aerodynamic performance improvements. The work described in this paper investigated multi-objective optimization to identify the possible tradeoffs between morphing airfoils with the least actuation energy and the lowest aerodynamic drag. This type of multi-objective optimization should be employed when studying candidate technologies for morphing aircraft.

To formulate the problem as a multi-objective problem, a strain energy model was developed that relied upon the concept of linearly elastic springs. This provided a straightforward calculation of the change in strain energy from one desired shape to another; however, it does not represent an actual morphing mechanism or strategy. As models of physically realizable mechanisms become available, these can provide a measure of actuation energy and should replace the linear spring energy model in the multi-objective formulation and solution approach presented here.

Before the multi-objective optimization was attempted, the morphing airfoil problem was solved using two aerodynamics-only problem formulations. In one formulation, a multipoint objective function was used to find the lowest energy airfoil. The solution to this problem is one fixed shape, so the strain energy associated with this is zero. In the other formulation, three single-point objective functions were used to find the morphing airfoil shapes that would represent the lowest-drag morphing airfoil. The solution to each of

the three problems seeks an airfoil shape with the lowest-drag coefficient at each flight condition. The multipoint solution and the single-point solution for the morphing airfoil shape bound the tradeoff between minimum energy and minimum drag.

Two multi-objective optimization approaches, both based upon the genetic algorithm, were used here to obtain representations of the Pareto-optimal set for the high-altitude, long-endurance aircraft-inspired problem. Both the ε-constraint and N-branch GA approaches identified tradeoff morphing airfoil designs that lie between the multipoint shape (lowest energy) and the set of single-point shapes (lowest drag). The worker–manager parallel implementation for the GA greatly reduced the elapsed time for the optimization from that needed from a serial implementation. The N-branch GA finds far more tradeoff designs than the ε-constraint approach with less computational effort.

The "compromise" designs from the Pareto sets show a significant reduction in energy from the single-point shape set, but these compromise designs have only a slight increase in drag from the single-point shape set. From these multi-objective results, engineers can then select a solution that gains the most improvement in aerodynamic performance for an acceptable level of actuation energy. Although the aerodynamic analyses and computational effort will be different, this approach appears amenable to morphing airfoil design across a broader regime of flight conditions (e.g., conditions that include subsonic, transonic and supersonic flow) and to three-dimensional morphing wing design, assuming a suitable actuation energy model is available.

Acknowledgments

A portion of this work was supported by the U.S. Air Force Research Laboratory Award F33615-00-C-3051. The calculations were performed on a 104-node cluster acquired by a Defense University Research Instrumentation Program (DURIP) Grant (DAAD19-01-1-0439) supported by the U.S. Army Research Office. The authors thank J. Bowman and B. Sanders of the U.S. Air Force Research Laboratory Air Vehicles Directorate, Wright–Patterson AFB, OH, for providing information about the high-altitude, long-endurance aircraft.

References

[1] McGowan, A. R., Washburn, A. E., Horta, L. G., Bryant, R. G., Cox, D. E., Siochi, E. J., Padula, S. L., and Holloway, N. M., "Recent Results from NASA's Morphing Project," SPIE Paper 4698-11, March 2002.

[2] Wlezien, R. W., Horner, G. C., McGowan, A. R., Padula, S. L., Scott, M. A., Silcox, R. J., and Simpson, J. O., "The Aircraft Morphing Program," AIAA Paper 1998-1927, April 1998.

[3] Wall, R., "Darpa Eyes Materials for 'Morphing' Aircraft," *Aviation Week and Space Technology*, Vol. 156, No. 14, April 2002, p. 36.

[4] Bowman, J., Sanders, B., and Weisshaar, T., "Evaluating The Impact of Morphing Technologies on Aircraft Performance," AIAA Paper 2002-1631, April 2002.

[5] Cesnik, C., Last, H., and Martin, C., "A Framework for Morphing Capability Assessment," AIAA Paper 2004-1654, April 2004.

[6] Renken, J. H., "Mission Adaptive Wing Camber Control Systems for Transport Aircraft," AIAA Paper 1985-5006, Oct. 1985.

[7] Kudva, J. N., Martin, C. A., Scherer, L. B., Jardine, A. P., McGowan, A. R., Lake, R. C., Sendecky, G. P., and Sanders, B. P., "Overview of the DARPA/AFRL/NASA Smart Wing Program," SPIE Paper 3674-26, March 1999.

[8] Pitt, D. M., Dunne, J. P., White, E. V., and Garcia, E., "SAMPSON Smart Inlet SMA Powered Adaptive Lip Design and Static Test," AIAA Paper 2001-1359, April 2001.

[9] Drela, M., "Pros & Cons of Airfoil Optimization," *Frontiers of Computational Fluid Dynamics—1998*, World Scientific Publishers, Singapore, 1998, pp. 363–381.

[10] Hicks, R. M., Murman, E. M., and Vanderplaats, G. N., "An Assessment of Airfoil Design by Numerical Optimization," NASA TM X-3092, July 1974.

[11] Vanderplaats, G. N., "CONMIN—A FORTRAN Program for Constrained Function Minimization, User's Manual," NASA TM X-62282, Aug. 1973, with addendum June 1978.

[12] Kennelly, R. A., "Improved Method for Transonic Airfoil Design-by-Optimization," AIAA Paper 1983-1864, July 1983.

[13] Jameson, A., "Aerodynamic Design via Control Theory," Institute for Computer Application in Science and Engineering, Rept. 88-64, NASA Langley Research Center, Hampton, VA, Nov. 1988.

[14] Holland, J. H., *Adaptation in Natural and Artificial Systems*, Univ. of Michigan Press, Ann Arbor, MI, 1974.

[15] Goldberg, D. E., *Genetic Algorithms in Search Optimization and Machine Learning*, Addison–Wesley, Reading, MA, 1989.

[16] Kirkpatrick, S., Gelatt, C. D., Jr., and Vecchi, M. P., "Optimization by Simulated Annealing," *Science*, Vol. 220, No. 4598, May 1983, pp. 671–680.

[17] Obayashi, S., and Tsukahara, T., "Comparison of Optimization Algorithms for Aerodynamic Shape Design," *AIAA Journal*, Vol. 35, No. 8, 1997, pp. 1413–1415.

[18] Holst, L. T., and Pulliam, H. T., "Aerodynamic Shape Optimization Using Real-Number-Encoded Genetic Algorithm," AIAA Paper 2001-2473, June 2001.

[19] Namgoong, H., Crossley, W. A., and Lyrintzis, A. S., "Issues for Global Optimization in Multipoint Transonic Airfoil Design," AIAA Paper 2002-5641, Sept. 2002.

[20] Maute, K., and Reich, G. W., "Integrated Multidisciplinary Topology Optimization Approach to Adaptive Wing Design," *Journal of Aircraft*, Vol. 43, No. 1, 2006, pp. 253–263.

[21] Lu, K.-J., and Kota, S., "Design of Compliant Mechanisms for Morphing Structural Shapes," *Journal of Intelligent Material Systems and Structures*, Vol. 14, No. 6, 2003, pp. 379–391.

[22] Reich, G. W., Bowman, C. J., and Sanders, B., "Large-Area Aerodynamic Control for High-Altitude Long-Endurance Sensor Platforms," *Journal of Aircraft*, Vol. 42, No. 1, 2005, pp. 237–244.

[23] Drela, M., "XFOIL: An Analysis and Design System for Low Reynolds Number Airfoils," *Low Reynolds Number Aerodynamics*, edited by T. J. Mueller, Vol. 54, Lecture Notes in Engineering, Springer–Verlag, Berlin, 1989, pp. 1–12.

[24] Namgoong, H., "Airfoil Optimization for Morphing Aircraft," Ph.D. Dissertation, School of Aeronautics and Astronautics, Purdue Univ., West Lafayette, IN, Dec. 2005.

[25] Hager, J. O., Eyi, S., and Lee, K. D., "Two-Point Transonic Airfoil Design Using Optimization for Improved Off-Design Performance," *Journal of Aircraft*, Vol. 31, No. 5, 1994, pp. 1143–1147.

[26] Hicks, R. M., and Henne, P. A., "Wing Design by Numerical Optimization," *Journal of Aircraft*, Vol. 15, No. 7, 1978, pp. 407–412.

[27] Prock, B. C., Weisshaar, T. A., and Crossley, W. A., "Morphing Airfoil Shape Change Optimization with Minimum Actuator Energy as an Objective," AIAA Paper 2002-5401, Sept. 2002.

[28] Nankani, K., "Optimization Approaches for Morphing Airfoils Using Drag and Strain Energy as Objectives," M.S. Thesis, School of Aeronautics and Astronautics, Purdue Univ., West Lafayette, IN, 2005.

[29] Maclean, B. J., Carpenter, B. F., Drape, J. L., and Misra, M. S., "A Compliant Wing Section for Adaptive Wing Surfaces," *Proceedings of the ADPA/AIAA/ASME/SPIE Conference on Active Materials*, edited by G. Knowles, Institute of Physics, Bristol, England, U.K., 1992, pp. 281–284.

[30] Saggere, L., and Kota, S., "Static Shape Control of Smart Structures Using Compliant Mechanisms," *AIAA Journal*, Vol. 37, No. 5, 1999, pp. 572–578.

[31] Martin, E. T., Hassan, R. A., and Crossley, W. A., "Comparing the N-Branch Genetic Algorithm and the Multi-Objective Genetic Algorithm," *AIAA Journal*, Vol. 42, No. 7, 2004, pp. 1495–1500.

[32] Crossley, W. A., Cook, A. M., Fanjoy, D. W., and Venkayya, V. P., "Using the Two-Branch Tournament Genetic Algorithm for Multiobjective Design," *AIAA Journal*, Vol. 37, No. 2, 1999, pp. 261–275.

[33] Fonseca, C., and Fleming, P., "Genetic Algorithms for Multiobjective Optimization: Formulation, Discussion and Generalization," *Proceedings of the Fifth International Conference on Genetic Algorithms*, edited by S. Forrest, Morgan Kaufmann, San Mateo, CA, 1993, pp. 416–423.

[34] Crossley, W. A., Nankani, K., and Raymer, D. P., "Comparison of Bit-String Affinity and Consecutive Generation Stopping Criteria for Genetic Algorithms," AIAA Paper 2004-0449, Jan. 2004.

[35] Williams, E. A., and Crossley, W. A., "Empirically-Derived Population Size and Mutation Rate Guidelines for a Genetic Algorithm with Uniform Crossover," *Soft Computing in Engineering Design and Manufacturing*, edited by P. K. Chawdhry, R. Roy, and R. K. Pant, Springer–Verlag, Berlin, 1998, pp. 163–172.

[36] Jones, B. R., Crossley, W. A., and Lyrintzis, A. S., "Aerodynamic and Aeroacoustic Optimization of Airfoils via a Parallel Genetic Algorithm," *Journal of Aircraft*, Vol. 37, No. 5, 2000, pp. 1088–1096.

[37] Sobieszczanski-Sobieski, J., and Haftka, R. T., "Multidisciplinary Aerospace Design Optimization: Survey of Recent Developments," *Structural Optimization*, Vol. 14, No. 1, 1997, pp. 1–23.

[38] Simpson, T. W., Peplinski, J., Koch, P. N., and Allen, J. K., "Metamodels for Computer-Based Engineering and Design: Survey and Recommendations," *Engineering with Computers*, Vol. 17, No. 2, 2001, pp. 129–150.

[39] Vincent, T., and Grantham, W., *Optimality in Parametric Systems*, 1st ed., Wiley, New York, 1981, pp. 72–103.

A. Messac
Associate Editor